molbank

MDPI

Communication

Revisiting the Coordination Chemistry of Molybdenum(V): Novel Complexes with Pyrazinoate and Picolinate Ligands

Barbara Modec * and Nina Podjed Rihtaršič

Faculty of Chemistry and Chemical Technology, University of Ljubljana, Večna pot 113, 1000 Ljubljana, Slovenia
* Correspondence: barbara.modec@fkkt.uni-lj.si

Abstract

Reactions of $(pyH)_5[MoOCl_4(H_2O)]_3Cl_2$ with picolinic and pyrazinoic acids yielded three new dinuclear molybdenum(V) complexes: $(pyH)_2[Mo_2O_4Cl_2(pic)_2]\cdot CH_3CN$ (**1**), $(pyH)_2[Mo_2O_4Cl_2(pic)_2]\cdot CH_3CH_2CN$ (**2**) and $(pyH)_2[Mo_2O_4Cl_2(pyraz)_2]\cdot CH_3CN$ (**3**) (pic^- = picolinate, $pyraz^-$ = pyrazinoate and pyH^+ = protonated pyridine). The compounds were characterized by single-crystal X-ray diffraction, infrared and ^1H NMR spectroscopy, elemental analysis, and TG/DSC measurements. All display a robust $\{Mo^V_2O_4\}^{2+}$ core with the heteroaromatic ligands bound in a *N*,*O*-bidentate chelating manner.

Keywords: molybdenum(V); picolinate; pyrazinoate; crystal structures

1. Introduction

In continuation of our studies on the $\{Mo^V_2O_4\}^{2+}$ coordination chemistry with quinaldinate (anionic form of quinoline-2-carboxylic acid, abbreviated as $quin^-$) [1], our investigation was extended to two related ligands: picolinate (pic^-) and pyrazinoate ($pyraz^-$). The structural formulae of the ligands are shown in Scheme 1, while Scheme 2 depicts the structure of the $\{Mo^V_2O_4\}^{2+}$ unit. The dinuclear unit dominates the coordination chemistry of molybdenum(V) [2–10]. Compounds containing this structural fragment often form unexpectedly across diverse ligand systems, owing to the remarkable stability of the $\{Mo^V_2O_4\}^{2+}$ core. Regardless of the ligand environment, its structural characteristics remain unchanged [2]. With the bridging unit being non-planar, the metal ions are brought into close proximity, with a typical separation of 2.5–2.6 Å. Such a distance is consistent with a direct bonding interaction between two d^1 ions, known as a single metal–metal bond [11]. Consequently, $\{Mo^V_2O_4\}^{2+}$ compounds are diamagnetic. Another characteristic of the $\{Mo^V_2O_4\}^{2+}$ structural fragment is the presence of two Mo=O bonds, which labilize bonds with ligands in their *trans* position. Overall, the dinuclear unit has six coordination sites that can accommodate a variety of *N*-, *O*- or *S*-donor ligands. In their absence, the coordination demands of molybdenum centers are met through aggregation into clusters, enabled by alkoxide and oxide ligands. In particular, the latter can adopt doubly, triply or even quadruply bridging roles [2,12]. Our previous reactions with quinaldinate yielded a discrete dinuclear anionic complex, $[Mo_2O_4(quin)_3]^-$ [1]. In this complex, quinaldinate ligands coordinated to the dinuclear unit in two distinctly different ways: two quinaldinates bound in the usual manner, i.e., as a *N*,*O*-bidentate chelating ligand to a single metal ion [13], whereas one adopted an *O*,*O*′-bridging fashion where carboxylate oxygens bound to separate metal ions. In the latter case, the carboxylate functioned as a third bridge between the metal ions thus forming a coordination motif frequently observed for carboxylate ligands in $\{Mo^V_2O_4\}^{2+}$ chemistry [14–16].

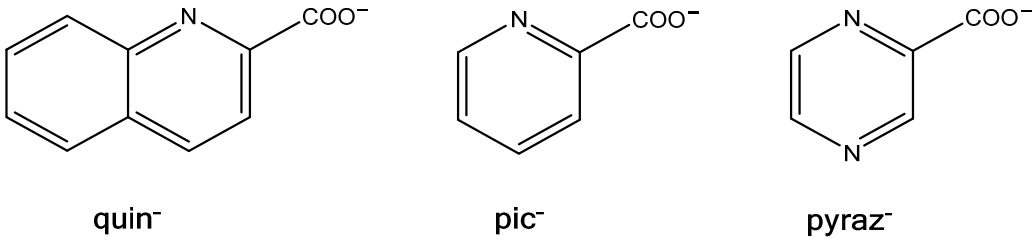
check for updates

Received: 6 October 2025
Revised: 21 October 2025
Accepted: 22 October 2025
Published: 24 October 2025

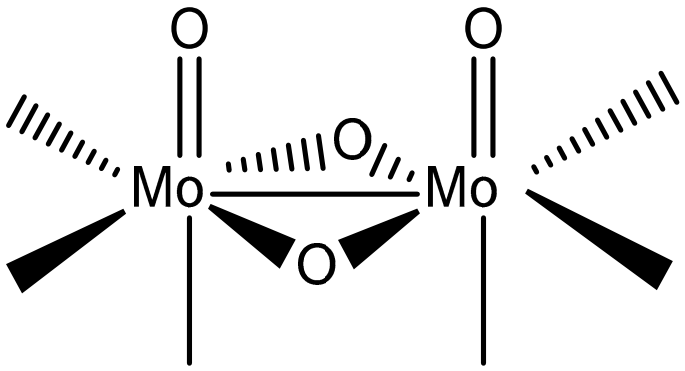
Citation: Modec, B.; Podjed Rihtaršič, N. Revisiting the Coordination Chemistry of Molybdenum(V): Novel Complexes with Pyrazinoate and Picolinate Ligands. *Molbank* **2025**, *2025*, M2079. https://doi.org/10.3390/M2079

Copyright: © 2025 by the authors. Licensee MDPI, Basel, Switzerland. This article is an open access article distributed under the terms and conditions of the Creative Commons Attribution (CC BY) license (https://creativecommons.org/licenses/by/4.0/).

The present study focuses on the products of the $(pyH)_5[MoOCl_4(H_2O)]_3Cl_2$ reactions with picolinic and pyrazinoic acid. Since picolinate shares the same donor set as quinaldinate, it was expected to behave analogously, although differences in solubility could influence reaction outcomes. Pyrazinoate, by contrast, offers greater structural versatility due to the presence of an additional nitrogen donor atom. Engagement of this site in coordination may lead to diverse bridging modes. Three novel crystalline compounds were obtained: $(pyH)_2[Mo_2O_4Cl_2(pic)_2]\cdot CH_3CN$ (**1**), $(pyH)_2[Mo_2O_4Cl_2(pic)_2]\cdot CH_3CH_2CN$ (**2**) and $(pyH)_2[Mo_2O_4Cl_2(pyraz)_2]\cdot CH_3CN$ (**3**) (pyH^+ stands for protonated pyridine). The molecular structures of **1** and **3** were determined by means of single-crystal X-ray diffraction analysis, whereas the identity of **2** was deduced from its infrared and ^1H NMR spectra, elemental analysis and TG/DSC analysis.



Scheme 1. Structural formulae of multidentate ligands discussed in this study.



Scheme 2. Structural formula of dinuclear $\{Mo^V_2O_4\}^{2+}$ unit showing its coordination sites.

2. Discussion

2.1. Synthetic Considerations

Reaction of the mononuclear $(pyH)_5[MoOCl_4(H_2O)]_3Cl_2$ in the mixture of acetonitrile and nitromethane with picolinic acid afforded a single product, crystalline $(pyH)_2[Mo_2O_4Cl_2(pic)_2]\cdot CH_3CN$ (**1**) of an orange-red color in a relatively good yield. The base, used for deprotonation of picolinic acid, was pyridine. In its absence, the reaction mixture retained its initial deep dark red, almost violet color and no solid could be isolated. An excess of the acid and base was used. The mononuclear $[MoOCl_4(H_2O)]^-$ ion underwent both substitution of the labile aqua and chloride ligands and dimerization, ultimately forming a stable $\{Mo^V_2O_4\}^{2+}$ structural core. The chloride substitution was not complete: one-fourth of chlorides remained coordinated. The synthetic procedure for compound **1** was modified by replacing acetonitrile with propionitrile. The substitution of nitrile solvent did not alter the reaction course as the analogous crystalline product, $(pyH)_2[Mo_2O_4Cl_2(pic)_2]\cdot CH_3CH_2CN$ (**2**), formed. In this compound, propionitrile molecules of crystallization fulfill the same role as acetonitrile in compound **1**. The formation of compounds **1** and **2** is summarized in the balanced equation shown below.

$$2\ (pyH)_5[MoOCl_4(H_2O)]_3Cl_2 + 6\ picH + 6\ py \rightarrow 3\ (pyH)_2[Mo_2O_4Cl_2(pic)_2] + 12\ HCl + 10\ pyHCl$$

For the formation of the analogous pyrazinoate compound, $(pyH)_2[Mo_2O_4Cl_2(pyraz)_2]\cdot CH_3CN$ (**3**), a different solvent system, namely a mixture of acetonitrile and methanol, can be used. In addition, pyridine was replaced with triethylamine as the base. The formation of compound **3** is summarized in the equation shown below.

$$2\ (pyH)_5[MoOCl_4(H_2O)]_3Cl_2 + 6\ pyrazH + 6\ Et_3N \rightarrow 3\ (pyH)_2[Mo_2O_4Cl_2(pyraz)_2] + 12\ HCl + 4\ pyHCl + 6\ Et_3NHCl$$

Our previous studies have shown that the use of methanol as a solvent typically results in the depletion of chloride ligands from the molybdenum(V) coordination sphere. Notably, this was not the case with the synthesis of $(pyH)_2[Mo_2O_4Cl_2(pyraz)_2]\cdot CH_3CN$ (**3**).

2.2. Crystal Structures

The crystal structures of $(pyH)_2[Mo_2O_4Cl_2(pic)_2]\cdot CH_3CN$ (**1**) and $(pyH)_2[Mo_2O_4Cl_2(pyraz)_2]\cdot CH_3CN$ (**3**) show pronounced similarities. Both compounds crystallize in triclinic space group *P* 1. Their solid-state structures consist of dinuclear complex anions, $[Mo_2O_4Cl_2(pic)_2]^{2-}$ in **1** and $[Mo_2O_4Cl_2(pyraz)_2]^{2-}$ in **3**, pyridinium ions as counter-cations and acetonitrile solvent molecules of crystallization. The ORTEP drawing of the dinuclear complex anions of **1** and **3** are shown in Figures 1 and 2. In the complex anions, the ligands, picolinate and pyrazinoate coordinate in a bidentate chelating manner through nitrogen and one carboxylate oxygen atom. The coordination environment of each molybdenum ion thus consists of three oxides and one chloride apart from the *N*- and *O*-donors of the picolinate/pyrazinoate. The $ClNO_4$ donor set occupies vertices of a highly distorted octahedron. The relative position of ligands in the complex anions is such that their symmetry closely approaches that of the C_2 point group with a two-fold rotation axis bisecting the Mo–Mo vector. The similarity between the two complex anions extends also to the bonding parameters. The relevant bonds and angles are given in Table 1. The Mo–Mo bonds amount 2.5704(6) Å in **1** and 2.5592(6) Å in **3** and as such fall within the typical range observed for $\{Mo^V{}_2O_4\}^{2+}$ compounds [2]. For instance, a very similar Mo–Mo bond length, namely 2.5682(3) Å, is observed in a quinaldinate complex $[Mo_2O_4(quin)_3]^-$ [1] whose metal ions are bridged in addition by two oxides also with a carboxylate moiety. On the other hand, the picolinate and pyrazinoate complexes display more bent $Mo(\mu_2\text{-}O)_2Mo$ bridging units than $[Mo_2O_4(quin)_3]^-$, as shown by the so-called "fold" angles, 151.1(2)° (in compound **1**) and 151.4(3)° (in **3**) vs. 163.36(16)° (in a quinaldinate complex). The picolinate/pyrazinoate ligands in $[Mo_2O_4Cl_2(pic)_2]^{2-}$/$[Mo_2O_4Cl_2(pyraz)_2]^{2-}$ have coordinated with the nitrogen donor occupying the site *cis* to the Mo=O moiety, whereas the carboxylate oxygen occupies the *trans* site. By contrast, the *N*,*O*-donors of the chelating quinaldinate ligands in $[Mo_2O_4(quin)_3]^-$ occupy positions that are both *cis* with respect to the Mo=O moiety. The comparison of the ligands' bond lengths is thus limited only to the nitrogen-to-molybdenum bonds and shows them to be very similar. Significant differences, as a result of the operating trans influence of the Mo=O moiety, may be observed in the carboxylate-to-molybdenum bonds: the Mo–O(carboxylate) bonds in **1** [2.155(5), 2.180(5) Å] and **3** [2.154(6), 2.202(6) Å] are longer than in $[Mo_2O_4(quin)_3]^-$ [2.0826(16), 2.0859(19) Å].

In the structures of **1** and **3**, the pyridinum cations are hydrogen-bonded to the complex anions. In both, one pyridinium cation is attached to one of the two bridging oxides, whereas the other pyridinium cation binds to the non-coordinated carboxylate oxygen of one of the two picolinates/pyrazinoates. Additionally, $\pi\cdots\pi$ interactions occur between pyridinium cations in the solid-state structure of **1**.

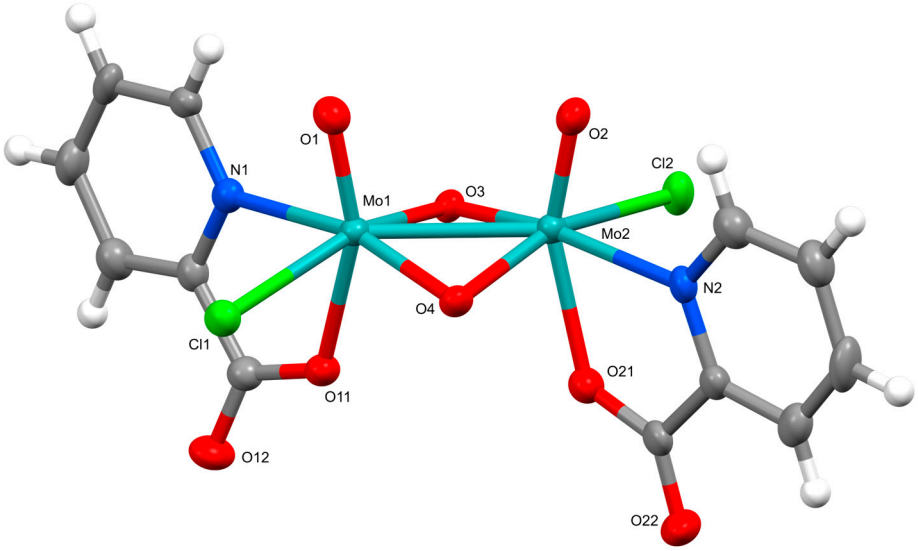


Figure 1. ORTEP drawing of the dinuclear complex in $(pyH)_2[Mo_2O_4Cl_2(pic)_2]\cdot CH_3CN$ (**1**). Thermal ellipsoids are drawn at the 50% probability level.

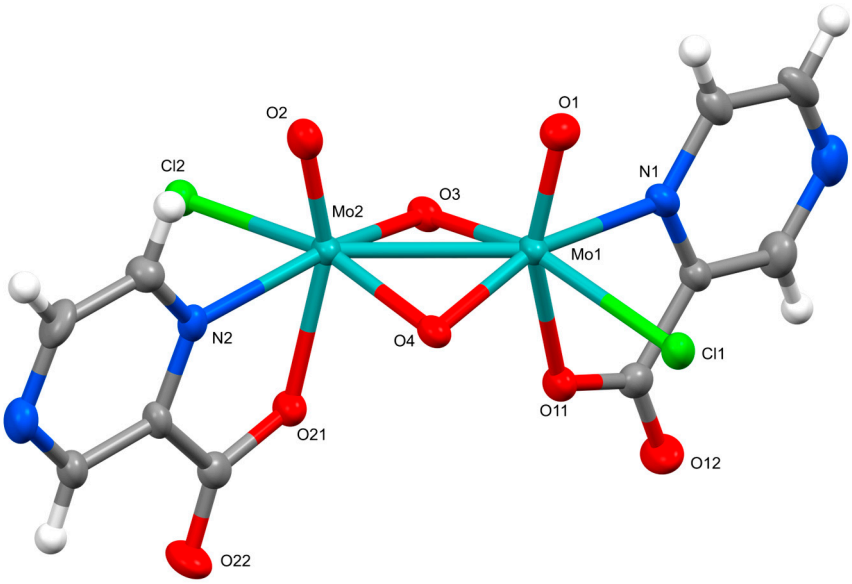


Figure 2. ORTEP drawing of the dinuclear complex in $(pyH)_2[Mo_2O_4Cl_2(pyraz)_2]\cdot CH_3CN$ (**3**). Thermal ellipsoids are drawn at the 50% probability level.

Table 1. Relevant geometric parameters [Å,°] in complex anions of **1** and **3**.

	$[Mo_2O_4Cl_2(pic)_2]^{2-}$ in **1**	$[Mo_2O_4Cl_2(pyraz)_2]^{2-}$ in **3**
Mo–Mo	2.5704(6)	2.5592(6)
"fold" angle *	151.1(2)	151.4(3)
Mo–Cl	2.4653(19), 2.4750(18)	2.4678(19), 2.469(2)
Mo–N	2.238(6), 2.254(6)	2.256(7), 2.271(7)
Mo–O(COO^-)	2.155(5), 2.180(5)	2.154(6), 2.202(6)

* Defined as a dihedral angle between two Mo(μ_2-O)$_2$ planes.

2.3. TG Analysis

In an oxidizing atmosphere up to 800 °C, all three compounds display very similar thermal behavior, consistent with their similar crystal structures. TG and DSC curves for $(pyH)_2[Mo_2O_4Cl_2(pic)_2]\cdot CH_3CN$ (**1**) and $(pyH)_2[Mo_2O_4Cl_2(pyraz)_2]\cdot CH_3CN$ (**3**) are shown in Figures 3 and 4, whereas those of $(pyH)_2[Mo_2O_4Cl_2(pic)_2]\cdot CH_3CH_2CN$ (**2**) form part of the Supplementary Materials. A detailed description is given only for **3**. A complex

multi-step decomposition process was revealed. The onset of the first step is at ca. 140 °C. It is completed by 230 °C and accounts for 16.33% of mass loss. This initial decomposition cannot be attributed solely to the release of nitrile solvent molecules, as the observed mass loss is significantly greater than the calculated acetonitrile content, 5.30%. Upon further heating, additional mass losses occur in two steps. The latter stage is highly exothermic (peak at ca. 430 °C) and corresponds to the formation of molybdenum(VI) oxide, calcd./found as follows: 37.18%/36.53%. Its mass remains constant within the 450–610 °C interval. At higher temperatures, molybdenum(VI) oxide begins to sublime, leading to a continuous decrease in the mass of the solid residue.

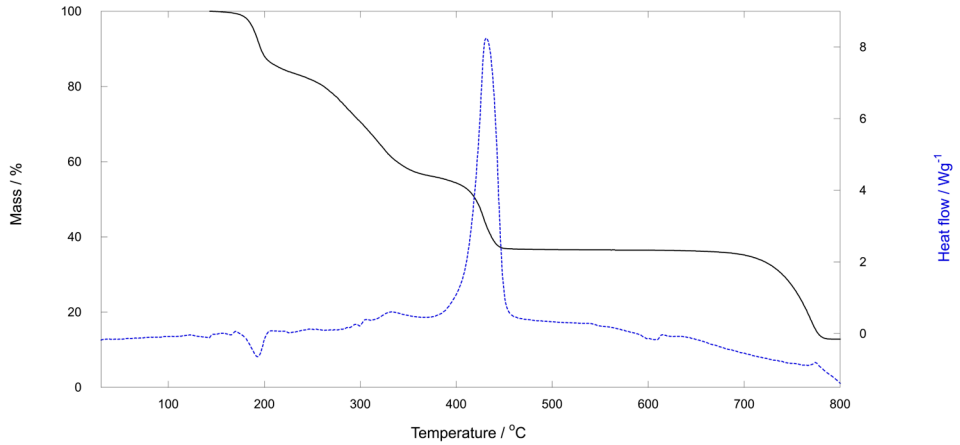


Figure 3. TG and DSC curves for $(pyH)_2[Mo_2O_4Cl_2(pyraz)_2]\cdot CH_3CN$ (**3**). The first region of mass loss starts at *ca*. 140 °C, followed by three more. The solid residue, 36.53% by mass, in the 460–610 °C temperature region is MoO_3 which sublimes at higher temperatures.

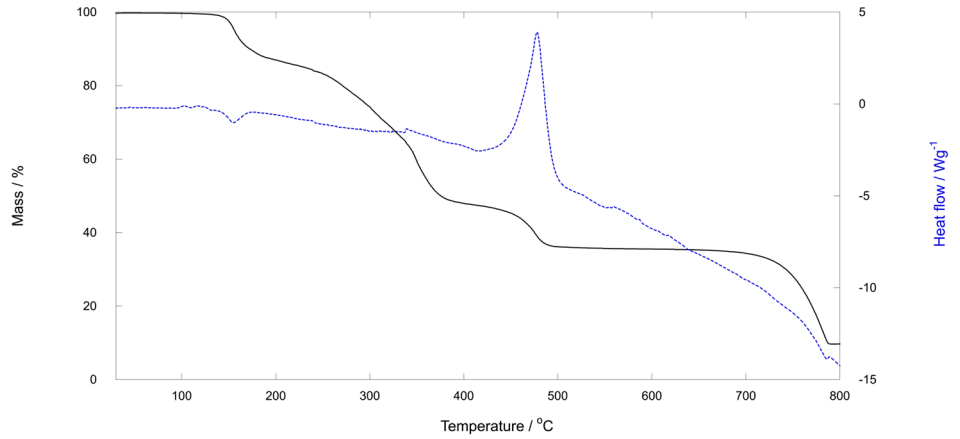


Figure 4. TG and DSC curves for $(pyH)_2[Mo_2O_4Cl_2(pic)_2]\cdot CH_3CN$ (**1**). The first region of mass loss starts at *ca*. 120 °C and is roughly completed by 210 °C. It accounts for 12.77% of the mass loss (the calculated content of acetonitrile is 5.31%). The solid residue, 35.59% by mass, in the 520–640 °C temperature region is MoO_3.

3. Experimental

3.1. General Remarks

Chemicals were purchased from Aldrich (St. Louis, MO, USA) and used as received. $(pyH)_5[MoOCl_4(H_2O)]_3Cl_2$ was prepared following the published procedure [17]. Microanalyses (C, H, N) were performed by the in-house facility on a Perkin–Elmer 2400 II instrument (Shelton, CT, USA). The infrared spectra were measured directly on solid samples using ATR with a Bruker Alpha II FTIR spectrometer (Rheinstetten, Germany). Spectra were obtained between 4000 and 400 cm^{-1} with 2 cm^{-1} resolution and 25 scans

and are shown as acquired without corrections or other manipulations. Spectra revealed characteristic absorption bands for vibrations of carboxylate [18] and terminal Mo=O groups [19]. TG-DSC measurements were performed on a Mettler Toledo TGA/DSC1 instrument (Schwerzenbach, Switzerland) in a temperature range from 25 to 800 °C with a heating rate of 5 K/min. During the measurement, the furnace was purged with synthetic air with a flow rate of 50 mL/min. 150 µL alumina crucible was used and the initial masses of the samples were around 10 mg. The blank curve was subtracted. Molybdenum content in the samples was determined as MoO_3, solid residue in the 450–630 °C temperature interval. ^{1}H NMR spectra of DMSO-d_6 solutions were obtained on a Bruker Avance NEO (Rheinstetten, Germany) at 600 MHz. The spectra were referenced to the central peak of the residual resonance for DMSO-d_6 at 2.50 ppm [20]. Chemical shifts (δ) are given in ppm, multiplicities are reported as follows: s = singlet, d = doublet, t = triplet, q = quartet and m = multiplet. Data were processed with MestReNova program (version 14.2.2) [21]. With the exception of the nitrile resonances, the ^{1}H NMR spectra of compounds **1** and **2** are essentially identical. Moreover, the number and the shape of the resonances associated with the picolinate (in compounds **1** and **2**) or pyrazinoate ligands (in **3**) strongly indicate the presence of exchange processes within the dinuclear complex anions. Nevertheless, in all three spectra, the sum of integrals is consistent with the compounds' composition, i.e., the molar ratio between the pyH^+ cations and the heteroaromatic ligands is 1:1.

3.2. X-Ray Crystallography

The crystals were mounted on the tip of a glass fiber with a small amount of silicon grease and transferred to a goniometer head. Data were collected on an Agilent SuperNova diffractometer (Oxfordshire, UK) with molybdenum (Mo-K_α, λ = 0.71073 Å) microfocus sealed X-ray source at 150 K. CrysAlis PRO [22] was used for data processing. Structures were solved with Olex^2 software (version 1.5) [23] using ShelXT (version 2018/3) [24] and refined with least square methods in ShelXL [25]. Anisotropic displacement parameters were determined for all non-hydrogen atoms. Hydrogen atoms were placed at calculated positions and were allowed to ride on their parent atoms. Figures depicting the structures were prepared using Mercury [26]. The crystallographic data were deposited to the CCDC and assigned the deposition numbers 2492841 (**1**) and 2492842 (**3**).

Crystal data for **1**, $C_{24}H_{23}Cl_2Mo_2N_5O_8$ (772.25 g mol^{-1}): triclinic *P* 1, a = 7.8948(2) Å, b = 8.7632(3) Å, c = 10.9092(4) Å, α = 96.103(3)°, β = 103.765(3)°, γ = 102.504(3)°, V = 705.69(4) Å^3, Z = 1, ρ_{calcd} = 1.817 g cm^{-3}, μ = 1.134 mm^{-1}; 11,929 reflections collected (5512 independent, R_{int} = 0.0341). The final residues were R = 0.0327, and wR_2 = 0.0766 [5167 reflections, $I > 2\sigma(I)$], and R = 0.0370, and wR_2 = 0.0798 [all data].

Crystal data for **3**, $C_{22}H_{21}Cl_2Mo_2N_7O_8$ (774.24 g mol^{-1}): triclinic *P* 1, a = 6.9296(3) Å, b = 10.0862(4) Å, c = 10.8704(3) Å, α = 105.379(3)°, β = 94.753(3)°, γ = 107.344(4)°, V = 688.35(5) Å^3, Z = 1, ρ_{calcd} = 1.868 g cm^{-3}, μ = 1.165 mm^{-1}; 11,260 reflections collected (5417 independent, R_{int} = 0.0269). The final residues were R = 0.0376, and wR_2 = 0.0876 [5099 reflections, $I > 2\sigma(I)$], and R = 0.0415, and wR_2 = 0.0919 [all data].

3.3. Preparation of $(pyH)_2[Mo_2O_4Cl_2(pic)_2]\cdot CH_3CN$ (**1**)

Picolinic acid (185 mg, 1.50 mmol) and pyridine (160 mg, 2.0 mmol) were added to the mixture of acetonitrile (15 mL) and nitromethane (10 mL). Afterwards, $(pyH)_5[MoOCl_4(H_2O)]_3Cl_2$ (214 mg, 0.50 mmol of Mo(V)) was added. The resulting mixture of a dark red color was stored in a closed Erlenmeyer flask under ambient conditions. Orange crystals of **1** were filtered off after 4 days. Yield: 145 mg; 75%. Found C, 36.98; H, 2.62; N, 9.08%. $C_{24}H_{23}Cl_2Mo_2N_5O_8$ (M = 772.25 g/mol) requires C, 37.33; H, 3.00%; N, 9.07%. TG determination of the Mo content, 23.7%. Required Mo, 24.9%. IR (ATR, cm^{-1}): 3083m [(C−H) in pic$^-$ and pyH^+], 2250w

[ν(C≡N) in CH_3CN], 1661vs, 1652vs, 1634vs, 1591vs [$\nu_{as}(COO^-)$ in pic^-], 1377vs, 1346vvs [$\nu_s(COO^-)$ in pic^-], 946vvs, 929vs [ν(Mo=O)]. ^{1}H NMR ($(CD_3)_2SO$ with 0.03% *v/v* TMS, 600 MHz): δ several resonances in the 9.36–7.19 range (m, 8H, pic^-), 8.88 (d, *J* = 5.0 Hz, 4H, pyH^+), 8.49 (t, *J* = 7.8 Hz, 2H, pyH^+), 7.99–7.96 (m, 4H, pyH^+), 2.07 (s, 3H, C*H*$_3$CN) ppm.

3.4. Preparation of (pyH)$_2$[Mo$_2$O$_4$Cl$_2$(pic)$_2$]·CH$_3$CH$_2$CN (**2**)

Picolinic acid (185 mg, 1.50 mmol) and pyridine (160 mg, 2.0 mmol) were added to the mixture of propionitrile (15 mL) and nitromethane (10 mL). Afterwards, $(pyH)_5[MoOCl_4(H_2O)]_3Cl_2$ (214 mg, 0.50 mmol of Mo(V)) was added. The resulting dark-red solution was stored in a closed Erlenmeyer flask under ambient conditions. Orange crystalline solid of **2** was filtered off after 4 days. Yield: 135 mg; 69%. Found C, 37.92; H, 3.05; N, 9.12%. $C_{25}H_{25}Cl_2Mo_2N_5O_8$ (*M* = 786.28 g/mol) requires C, 38.19; H, 3.20%; N, 8.91%. TG determination of the Mo content, 23.5%. Required Mo, 24.4%. IR (ATR, cm^{-1}): 3083m [(C−H) in pic^- and pyH^+], 2246w [ν(C≡N) in CH_3CH_2CN], 1661vs, 1633vs, 1590vs [$\nu_{as}(COO^-)$ in pic^-], 1378vs, 1345vvs [$\nu_s(COO^-)$ in pic^-], 946vvs, 928vs [ν(Mo=O)]. ^{1}H NMR ($(CD_3)_2SO$ with 0.03% *v/v* TMS, 600 MHz): δ several resonances in the 9.36–7.22 range (m, 8H, pic^-), 8.89 (d, *J* = 5.2 Hz, 4H, pyH^+), 8.51 (t, *J* = 7.7 Hz, 2H, pyH^+), 8.01–7.98 (m, 4H, pyH^+), 2.46 (q, *J* = 7.6 Hz, 2H, CH_3CH_2CN), 1.14 (t, *J* = 7.6 Hz, 3H, CH_3CH_2CN) ppm.

3.5. Preparation of (pyH)$_2$[Mo$_2$O$_4$Cl$_2$(pyraz)$_2$]·CH$_3$CN (**3**)

$(pyH)_5[MoOCl_4(H_2O)]_3Cl_2$ (214 mg, 0.50 mmol of Mo(V)) was dissolved in the mixture of acetonitrile (10 mL) and methanol (5 mL). To this solution, pyrazinoic acid (140 mg, 1.13 mmol) and triethylamine (0.33 mL, 2.37 mmol) were added. The resulting mixture of a brown-red color was stored in a closed Erlenmeyer flask under ambient conditions. Orange-red crystalline solid **3** was filtered off on the following day. Yield: 142 mg; 73%. Single crystals of **3** (used for X-ray structure analysis) were obtained from a slightly modified reaction mixture. Pyrazinoic acid (143 mg, 1.15 mmol) and pyridine (120 mg, 1.50 mmol) were added to the mixture of acetonitrile (10 mL), methanol (5 mL) and nitromethane (10 mL). Afterwards, $(pyH)_5[MoOCl_4(H_2O)]_3Cl_2$ (161 mg, 0.39 mmol of Mo(V)) was added. The resulting mixture was stored in a closed Erlenmeyer flask under ambient conditions. Within a couple hours, all the solids were consumed and the color of the solution changed to orange-red. On the following day, large orange crystals of **3** were obtained.

The crystalline solids obtained from both preparations exhibit identical infrared spectra. Found C, 34.12; H, 2.59; N, 12.52%. $C_{22}H_{21}Cl_2Mo_2N_7O_8$ (*M* = 774.24 g/mol) requires C, 34.13; H, 2.73%; N, 12.66%. TG determination of the Mo content, 24.4%. Required Mo, 24.8%. IR (ATR, cm^{-1}): 3071m, 3057m [ν(C−H) in $pyraz^-$ and pyH^+], 2247w [ν(C≡N) in CH_3CN], 1666vvs, 1634vvs [$\nu_{as}(COO^-)$ in $pyraz^-$], 1375vvs, 1333vvs [$\nu_s(COO^-)$ in $pyraz^-$], 949vvs, 928vvs [ν(Mo=O)]. ^{1}H NMR ($(CD_3)_2SO$ with 0.03% *v/v* TMS, 600 MHz): δ several resonances in the 9.38–8.80 range (m, 6H, $pyraz^-$), 8.83 (d, *J* = 4.9 Hz, 4H, pyH^+), 8.37 (t, *J* = 7.8 Hz, 2H, pyH^+), 7.89–7.86 (m, 4H, pyH^+), 2.07 (s, 3H, C*H*$_3$CN) ppm.

4. Conclusions

Reactions of the mononuclear $(pyH)_5[MoOCl_4(H_2O)]_3Cl_2$ with either picolinic or pyrazinoic acid resulted in the analogous dinuclear $[Mo_2O_4Cl_2(pic)_2]^{2-}$ and $[Mo_2O_4Cl_2(pyraz)_2]^{2-}$ complexes which retained some chloride ligands and had their heteroaromatic ligands bound in a *N*,*O*-bidentate chelating manner. The coordination behavior of picolinate and pyrazinoate contrasts with that of the similar quinaldinate which was bound also via its carboxylate moiety in a *O*,*O*′-bidentate bridging manner. Notably, pyrazinoate did not fully exploit its coordination potential as its second nitrogen atom did not participate in bonding interactions with molybdenum.

Supplementary Materials: The following supporting information are available. Figure S1. Molecular structure of $(pyH)_2[Mo_2O_4Cl_2(pic)_2]\cdot CH_3CN$ (**1**); Figure S2. Molecular structure of $(pyH)_2[Mo_2O_4Cl_2(pyraz)_2]\cdot CH_3CN$ (**3**); Figure S3. Packing of ions and acetonitrile solvent molecules in $(pyH)_2[Mo_2O_4Cl_2(pic)_2]\cdot CH_3CN$ (**1**), as viewed along *b* axis; Figure S4. Packing of ions and acetonitrile solvent molecules in $(pyH)_2[Mo_2O_4Cl_2(pyraz)_2]\cdot CH_3CN$ (**3**), as viewed along b axis; Figure S5. TG and DSC curves for $(pyH)_2[Mo_2O_4Cl_2(pic)_2]\cdot CH_3CH_2CN$ (**2**); Figure S6. Infrared spectrum of $(pyH)_2[Mo_2O_4Cl_2(pic)_2]\cdot CH_3CN$ (**1**); Figure S7. Infrared spectrum of $(pyH)_2[Mo_2O_4Cl_2(pic)_2]\cdot CH_3CH_2CN$ (**2**); Figure S8. Infrared spectrum of $(pyH)_2[Mo_2O_4Cl_2(pyraz)_2]\cdot CH_3CN$ (**3**); Figure S9. ^1H NMR spectrum of $(pyH)_2[Mo_2O_4Cl_2(pic)_2]\cdot CH_3CN$ (**1**) in DMSO-d_6; Figure S10. ^1H NMR spectrum of $(pyH)_2[Mo_2O_4Cl_2(pic)_2]\cdot CH_3CH_2CN$ (**2**) in DMSO-d_6; Figure S11. ^1H NMR spectrum of $(pyH)_2[Mo_2O_4Cl_2(pyraz)_2]\cdot CH_3CN$ (**3**) in DMSO-d_6.

Author Contributions: Conceptualization, B.M. and N.P.R.; investigation, B.M. and N.P.R.; writing—review and editing, B.M. and N.P.R.; visualization, B.M. and N.P.R.; project administration, B.M. All authors have read and agreed to the published version of the manuscript.

Funding: This work was funded by the Slovenian Research and Innovation Agency (Research Core Funding Grant P1-0134). The authors acknowledge the support of the Centre for Research Infrastructure at the University of Ljubljana, Faculty of Chemistry and Chemical Technology, which is part of the Network of Research and Infrastructural Centres UL (MRIC UL) and is financially supported by the Slovenian Research and Innovation Agency (Infrastructure program No. I0-0022).

Data Availability Statement: The original contributions presented in this study are included in the article/Supplementary Material. Further inquiries can be directed to the corresponding author.

Acknowledgments: The authors thank Patrik Horžen, an undergraduate student at the time, for checking the reproducibility of the synthetic procedures.

Conflicts of Interest: The authors declare no conflicts of interest.

References

1. Modec, B.; Podjed, N.; Šturm, J. Oxidation *vs.* coordination chemistry of the $\{Mo^V_2O_4\}^{2+}$ species: A structural study. *J. Mol. Struct.* **2022**, *1253*, 132246. [CrossRef]
2. Chae, H.K.; Klemperer, W.G.; Marquart, T.A. High-nuclearity oxomolybdenum(V) complexes. *Coord. Chem. Rev.* **1993**, *128*, 209–224. [CrossRef]
3. Majumdar, M.; Patra, S.K.; Bera, J.K. Oxidative route to polyoxomolybdates from quadruply bonded $[Mo^{II}Mo^{II}]$ precursor: Structural characterization of a tetranuclear cluster $[Mo_4Cl_5O_8(pyNP)_2]$ (pyNP=(2-(2-pyridyl)1,8-naphthyridine)). *Polyhedron* **2007**, *26*, 1597–1602. [CrossRef]
4. Aguado, R.; Escribano, J.; Pedrosa, M.R.; De Cian, A.; Sanz, R.; Arnáiz, F.J. Binuclear oxomolybdenum(V) chlorides: Molecular structure of $Mo_2O_4Cl_2(DMF)_4$ and $Mo_2O_4Cl_2(bipy)_2\cdot DMF$. *Polyhedron* **2007**, *26*, 3842–3848. [CrossRef]
5. Lyashenko, G.; Herbst-Irmer, R.; Jancik, V.; Pal, A.; Mösch-Zanetti, N.C. Molybdenum oxo and imido complexes of β-diketiminate ligands: synthesis and structural aspects. *Inorg. Chem.* **2008**, *47*, 113–120. [CrossRef]
6. Modec, B.; Dolenc, D.; Kasunič, M. Complexation of molybdenum(V) with glycolic acid: An unusual orientation of glycolato ligand in $\{Mo_2O_4\}^{2+}$ complexes. *Inorg. Chem.* **2008**, *47*, 3625–3633. [CrossRef]
7. Compain, J.-D.; Dolbecq, A.; Marrot, J.; Mialane, P.; Sécheresse, F. Characterization of tetra, dodeca and tetradeca Mo^V polyoxometalate wheels structured by etidronate ligands. *C. R. Chimie* **2010**, *13*, 329–335. [CrossRef]
8. Mota Merelo de Aguiar, S.R.; Stöger, B.; Weil, M.; Kirchner, K. Tetrakis(μ_2-diphenylphosphinato-κ^2O,O')tetra-μ_3-oxido-tetraoxidohexamolybdenum(V). *IUCrData* **2016**, *1*, x160036. [CrossRef]
9. Gomes, A.C.; Neves, P.; Cunha-Silva, L.; Valente, A.A.; Gonçalves, I.S.; Pillinger, M. Oxidomolybdenum complexes for acid catalysis using alcohols as solvents and reactants. *Catal. Sci. Technol.* **2016**, *6*, 5207–5218. [CrossRef]
10. Wang, S.-Y.; Jin, W.-T.; Chen, H.-B.; Zhou, Z.-H. Comparison of hydroxycarboxylato imidazole molybdenum(IV) complexes and nitrogenase protein structures: Indirect evidence for the protonation of homocitrato FeMo-cofactors. *Dalton Trans.* **2018**, *47*, 7412–7421. [CrossRef]
11. Cotton, F.A.; Morehouse, S.M. The molecular structure of a diamagnetic, doubly oxygen-bridged, binuclear complex of molybdenum(V) containing a metal-metal bond. *Inorg. Chem.* **1965**, *4*, 1377–1381. [CrossRef]

12. Modec, B.; Brenčič, J.V. From small $\{Mo_2O_4\}^{2+}$ aggregates to infinite solids. *J. Cluster Sci.* **2002**, *13*, 279–302. [CrossRef]
13. Groom, C.R.; Bruno, I.J.; Lightfoot, M.P.; Ward, S.C. The Cambridge Structural Database. *Acta Crystallogr. Sect. B* **2016**, *72*, 171–179. [CrossRef]
14. Modec, B.; Dolenc, D.; Brenčič, J.V. New molybdenum(V) complexes based on the $\{Mo_2O_4\}^{2+}$ structural core with esters or anions of malonic and succinic acid. *Inorg. Chim. Acta* **2007**, *360*, 663–678. [CrossRef]
15. Ma, P.; Hu, F.; Wang, J.; Niu, J. Carboxylate covalently modified polyoxometalates: From synthesis, structural diversity to applications. *Coord. Chem. Rev.* **2019**, *378*, 281–309. [CrossRef]
16. Delaporte, S.; Abánades Lázaro, I.; López-Cabrelles, J.; Mazarakioti, E.C.; Chebourou, S.; Vitórica-Yrezábal, I.J.; Giménez-Marqués, M.; Mínguez Espallargas, G. Imparting structural robustness of metal–organic cages based on oxo-dimolybdenum clusters. *Dalton Trans.* **2023**, *52*, 15682–15687. [CrossRef]
17. Modec, B.; Brenčič, J.V. Novel methanol-containing oxomolybdate(V) complexes: Synthesis and structural characterisation of intermediates in the formation of $\{Mo_2O_4\}^{2+}$ clusters from $[MoOCl_4(H_2O)]^-$ and $[MoOBr_4]^-$ precursors. *Eur. J. Inorg. Chem.* **2005**, *2005*, 1698–1709. [CrossRef]
18. Deacon, G.B.; Phillips, R.J. Relationships between the carbon-oxygen stretching frequencies of carboxylato complexes and the type of carboxylate coordination. *Coord. Chem. Rev.* **1980**, *33*, 227–250. [CrossRef]
19. Heinze, K.; Fischer, A. Polymer-supported dioxido-Mo^{VI} complexes as truly functional molybdenum oxotransferase model systems. *Eur. J. Inorg. Chem.* **2007**, *2007*, 1020–1026. [CrossRef]
20. Gottlieb, H.E.; Kotlyar, V.; Nudelman, A. NMR chemical shifts of common laboratory solvents as trace impurities. *J. Org. Chem.* **1997**, *62*, 7512–7515. [CrossRef] [PubMed]
21. Willcott, M.R. MestRe Nova. *J. Am. Chem. Soc.* **2009**, *131*, 13180. [CrossRef]
22. Agilent. *CrysAlis PRO*; Agilent Technologies Ltd.: Yarnton, UK, 2014.
23. Dolomanov, O.V.; Bourhis, L.J.; Gildea, R.J.; Howard, J.A.K.; Puschmann, H. *Olex2*: A complete structure solution, refinement and analysis program. *J. Appl. Crystallogr.* **2009**, *42*, 339–341. [CrossRef]
24. Sheldrick, G.M. *SHELXT*—Integrated space-group and crystal-structure determination. *Acta Crystallogr. Sect. A* **2015**, *71*, 3–8. [CrossRef]
25. Sheldrick, G.M. Crystal structure refinement with *SHELXL*. *Acta Crystallogr. Sect. C* **2015**, *71*, 3–8. [CrossRef] [PubMed]
26. Macrae, C.F.; Sovago, I.; Cottrell, S.J.; Galek, P.T.A.; McCabe, P.; Pidcock, E.; Platings, M.; Shields, G.P.; Stevens, J.S.; Towler, M.; et al. *Mercury 4.0*: From visualization to analysis, design and prediction. *J. Appl. Cryst.* **2020**, *53*, 226–235. [CrossRef] [PubMed]

Disclaimer/Publisher's Note: The statements, opinions and data contained in all publications are solely those of the individual author(s) and contributor(s) and not of MDPI and/or the editor(s). MDPI and/or the editor(s) disclaim responsibility for any injury to people or property resulting from any ideas, methods, instructions or products referred to in the content.